Available online at www.sciencedirect.com
ScienceDirect
Journal of Power Sources 161 (2006) 346–355
JOURNAL OF POWER SOURCES
www.elsevier.com/locate/jpowsour

A thermally coupled metal hydride hydrogen storage and fuel cell system

Brendan D. MacDonald *, Andrew M. Rowe

Institute for Integrated Energy Systems, Department of Mechanical Engineering, University of Victoria, P.O. Box 3055 STN CSC, Victoria, BC, Canada V8W 3P6

Received 20 January 2006; received in revised form 31 March 2006; accepted 3 April 2006
Available online 22 May 2006

Abstract

This paper examines the ability of metal hydride storage systems to supply hydrogen to a fuel cell with a time varying demand, when the metal hydride tanks are thermally coupled to the fuel cell. A two-dimensional mathematical model is utilized to compare different heat transfer enhancements and storage tank configurations. The scenario investigated involves two metal hydride tanks containing the alloy $Ti_{0.98}Zr_{0.02}V_{0.43}Fe_{0.09}Cr_{0.05}Mn_{1.5}$, located in the air exhaust stream of a fuel cell. Three cases are simulated: a base case with no heat transfer enhancements, a case with external fins attached to the outside of the tank, and a case where an annular tank design is used. For the imposed duty cycle, the base case is insufficient to provide the hydrogen demands of the system, while both the finned and annular cases are able to meet the demands. The finned case yields higher pressures and occupies more space, while the annular case yields acceptable pressures and requires less space. Furthermore, the annular metal hydride tank meets the requirements of the fuel cell while providing a more robust and compact hydrogen storage system.

Keywords: Hydrogen storage; Metal hydride; Fuel cell; Heat transfer; Dynamic model

1. Introduction

Hydrogen storage in reversible metal hydrides is desirable because the hydrogen can be stored at low pressures with a high volumetric density. Hydrogen storage in metal hydrides is particularly advantageous for stationary or small-scale fuel cell applications, where the desire for small storage tanks outweighs the disadvantages of metal hydride mass.

A significant issue for metal hydride storage systems is limited heat transfer between the fluid on the exterior of the tank and the metal hydride alloy within the tank, at the location where the reaction is taking place. Often, the heat transfer rate is the controlling variable that determines the rate at which hydrogen gas can be extracted from a tank [1]. Increasing heat transfer rates is important for optimizing the design of metal hydride hydrogen storage applications.

Previous numerical studies of metal hydride storage tanks have focused on developing models to simulate various scenarios. One such study, preformed by Jiang et al. [2], investigated the behaviour associated with a thermally coupled hydrogen storage and fuel cell system. This work utilized a computational environment referred to as the virtual test bed to simulate the behaviour associated with uncoupled systems versus coupled systems. This model uses lumped approximations, and a pulsed hydrogen demand load was applied. Another study, performed by Mazumdar et al. [3], developed a one-dimensional mathematical model of a compressor driven metal hydride cooling system. This model takes into account transient characteristics of metal hydride reactors that are thermally coupled to each other, and includes external fins for heat transfer enhancement. Demircan et al. [4], experimentally validated a two-dimensional mathematical model for various bed geometries and configurations. This work concluded that there was reasonable agreement between the numerical results and experimental data for a cylindrical storage vessel as well as an annular storage vessel, when the tanks are charged by hydrogen provided at a constant pressure.

These studies improve the understanding of metal hydride storage systems but there is outstanding work that still remains. For example, thermal time constants could be better understood, time dependent loads could be further investigated for various scenarios, and an analysis of how to appropriately capture the waste exhaust heat from a fuel cell in thermally coupled situ-

* Corresponding author. Tel.: +1 250 7218920; fax: +1 250 7216051.
E-mail address: bdmacdon@uvic.ca (B.D. MacDonald).

0378-7753/$ – see front matter © 2006 Elsevier B.V. All rights reserved.
doi:10.1016/j.jpowsour.2006.04.018

Nomenclature

A_f	surface area of each fin (m^2)
A_o	area of the interior tube opening (m^2)
A_{side}	surface area of the side of the tank (m^2)
A_t	total area including base and fins (m^2)
c_{pa}	specific heat of the air ($J\,kg^{-1}\,K^{-1}$)
D	diameter of the tank (m)
D_o	diameter of the interior tube opening (m)
f	friction factor
g	acceleration due to gravity ($m\,s^{-2}$)
h_{base}	heat transfer coefficient for the base case ($W\,m^{-2}\,K^{-1}$)
h_{fin}	effective heat transfer coefficient for the finned wall ($W\,m^{-2}\,K^{-1}$)
h_n	heat transfer coefficient during the off-cycle ($W\,m^{-2}\,K^{-1}$)
h_{si}	heat transfer coefficient in the interior tube ($W\,m^{-2}\,K^{-1}$)
h_{side}	heat transfer coefficient over the side wall ($W\,m^{-2}\,K^{-1}$)
k	thermal conductivity of the air ($W\,m^{-1}\,K^{-1}$)
L	length of the inner tube (m)
m_a	mass flow rate of air ($kg\,s^{-1}$)
N	number of fins
Nu_∞	Nusselt number for fully developed flow
Nu_D	Nusselt number
Nu_m	mean Nusselt number for the entry region
P	perimeter (m)
Pr	Prandtl number
r	radius (m)
Ra_D	Rayleigh number
Re_D	Reynolds number
t	time (s)
T_∞	ambient air temperature (K)
T_a	air temperature as it exits the stack (K)
T_{air}	average air temperature (K)
T_f	film temperature (K)
T_{in}	air temperature prior to encountering the tank (K)
T_{out}	air temperature after encountering the tank (K)
T_s	surface temperature of the metal hydride tank (K)
T_{si}	local temperature of the interior tube wall (K)
T_{side}	temperature of the side of the tank (K)
T_{ss}	steady-state temperature (K)
T_0	initial temperature (K)
T_∞	ambient air temperature (K)
v_m	mean velocity of the air stream ($m\,s^{-1}$)
z	height (m)

Greek letters

α	thermal diffusivity ($m^2\,s^{-1}$)
η_f	fin efficiency
μ_a	dynamic viscosity of the air ($N\,s\,m^{-2}$)
ν	kinematic viscosity ($m^2\,s^{-1}$)
ρ_a	density of the air ($kg\,m^{-3}$)

ations should be performed. This study aims to address these issues by comparing different heat transfer enhancing configurations for a thermally coupled, metal hydride hydrogen storage and fuel cell system when a pulsed hydrogen load is applied. Aspects from all three of the above noted studies [2–4] will be combined and compared in this paper. The investigation will utilize a thermally coupled metal hydride and fuel cell system to compare a storage tank with no heat transfer enhancements to tanks with heat transfer enhancements in the form of external fins and an annular tank design.

There have been several mathematical models reported in the literature that simulate the dynamic behaviour of metal hydride reactors [2–12]. Jemni and Ben Nasrallah [7–10] have done considerable work developing two-dimensional models. The metal hydride model used in this work is based upon a previous study [12], and is similar to the models developed by Jemni and Ben Nasrallah [7–10]. For the current study, the previous model is expanded to include subdomains describing the tank walls and an external flow field representing the fuel cell exhaust air stream. It is implemented in a finite element program called COMSOL Multiphysics™.

2. System configuration

The fuel cell selected for this study is the BALLARD® Nexa™ power module. The Nexa™ is a commercial proton exchange membrane (PEM) fuel cell system capable of 1200 W peak power. For this study, it is assumed that the system is servicing an intermittent load cycling at levels of 0 and 50% power with a 30 min period. The complete load profile is thus 600 W of power for 15 min (on-cycle), shut-off for 15 min (off-cycle), and repeated for five complete cycles. The fuel cell is supplied hydrogen from two metal hydride canisters; therefore, the hydrogen demand is assumed to be equally divided between each tank. The hydrogen mass flow associated with this load is illustrated in Fig. 1 along with the state of fill of each hydride tank over the 2.5 h of pulsed operation. The waste heat provided by the

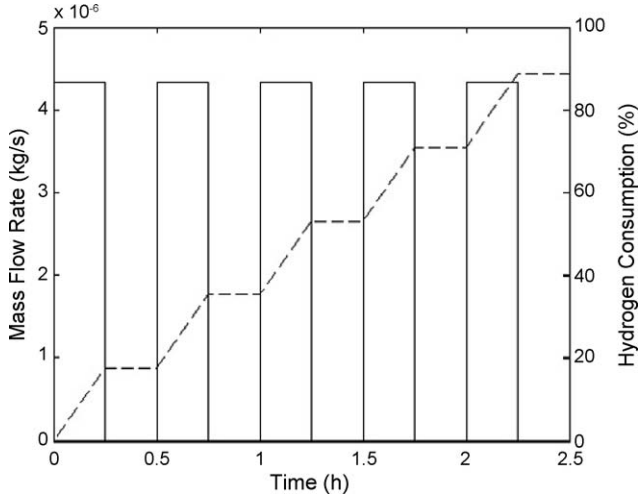

Fig. 1. Hydrogen mass flow rate exiting the tank and cumulative percentage of hydrogen in the metal hydride bed consumed over the 2.5 h of pulsed operation.

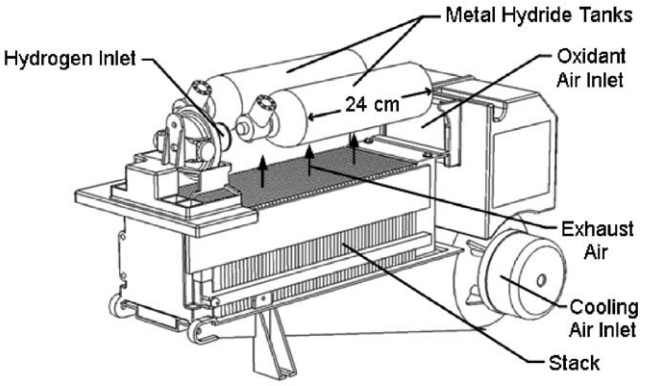

Fig. 2. Schematic of the system configuration illustrating the placement of two metal hydride tanks above the fuel cell's vertical cooling channels.

fuel cell module for a 600 W load is 550 W [13]. The tanks are thermally coupled to the fuel cell system by placement immediately above the vertical cooling channels, and additional duct work is used to ensure the waste heat air stream passes over the desired region or through the tank as required for each particular case. Fig. 2 shows the arrangement of the tanks relative to the fuel cell, and Fig. 3 shows the ducting work associated with the cases where the air flows over the exterior of the tanks. For the annular tanks, it is assumed that a collection manifold routes the exhaust gas through the inside of the storage tanks.

A previous study performed by the authors [12] utilized the AB_5 type alloy $LaNi_5$ while investigating the effect of external fins on an uncoupled system. The pressure provided by this alloy at temperatures in the ambient range is insufficient to provide hydrogen to the fuel cell, which requires a minimum inlet pressure of 170 kPa (absolute) [13]. For this study, a commercially available AB_2 type alloy, $Ti_{0.98}Zr_{0.02}V_{0.43}Fe_{0.09}Cr_{0.05}Mn_{1.5}$, is selected. The properties for this material are obtained from Sandrock [1]. The alloy has sufficiently high pressures in the ambient temperature range, a hydrogen storage capacity of 1.9 wt.%, and is inexpensive [1]. The size of the tanks is based upon the 20G250B model that is sold by Ovonic Hydrogen Systems LLC, which has a hydrogen capacity of 22 g, a diameter of 6.35 cm, and an approximate height of 26.5 cm including the valve [14].

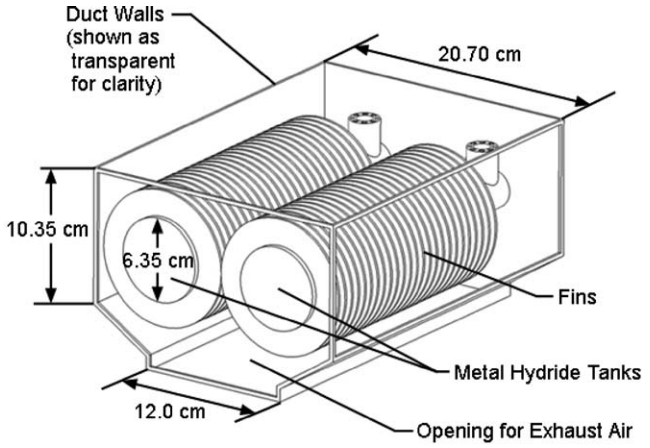

Fig. 3. Schematic of the ducting required for the finned configuration (note: not all fins are shown).

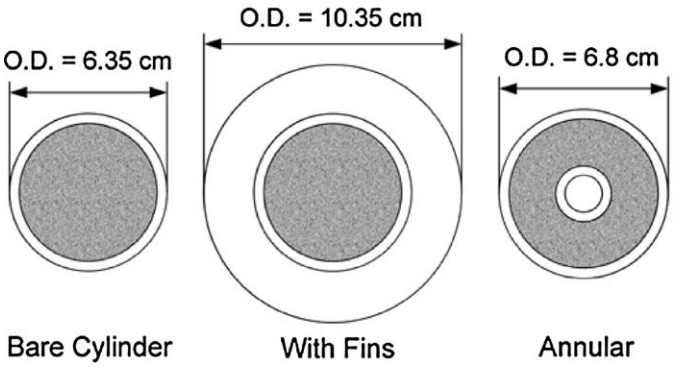

Fig. 4. Cross section of the metal hydride vessels for each of the three cases being studied, including a comparison of the outer diameter for each case.

In order to compare the heat transfer enhancements, three different cases are simulated. The first case is the base case, where no heat transfer enhancements are used. For the second case, the tank has 50 external fins of 2 cm length and 1 mm thickness attached on the circumference. The third case is an annular tank design where the air stream is piped directly through the centre of the tank. The annular geometry has an equivalent alloy content as the base case, but has a smaller overall diameter than the finned tank. Fig. 4 shows a cross section of each of the three cases with the corresponding outer diameters. Since both tanks in each scenario operate under similar conditions, the numerical model simulates one tank utilizing half of the waste heat air stream from the fuel cell.

3. Experimental data

In order to accurately represent the coupling between the metal hydride tanks and the fuel cell module some experimental data is required. Some data is available for the Nexa™ module running at rated output (1200 W). Since this study assumes operation of the fuel cell at 50% power (600 W), experimental data is used to more accurately characterize the temperature of the exhaust air.

The experiment involved the fuel cell started from off mode in equilibrium with the laboratory temperature and immediately set for an output load of 600 W. A thermocouple placed approximately 2 cm above the exhaust channels recorded air temperature while a sensor built into the fuel cell reported stack temperature. This experiment yielded a steady-state exhaust air temperature that is approximately 14 °C above ambient temperature. The time to reach steady-state yielded a thermal time constant, τ_{on}, of ~120 s. The recorded data is plotted in Fig. 5 as a dashed line.

After steady-state was reached the fuel cell was shut off, and the temperature of the fuel cell stack was recorded as it declined. This yielded a thermal time constant for the off-cycle, τ_{off}, of ~110 s. It can be seen from Fig. 5 that the experimental curve for the off-cycle is not a smooth line, and there is a distinct plateau reached at approximately 200 s before the temperature continues to decay towards ambient temperature. This behaviour is caused by the "purge cycle" of the fuel cell module. When the fuel cell is shut-off after operating at sufficiently high power loads it enters into a "purge cycle" lasting a few minutes where

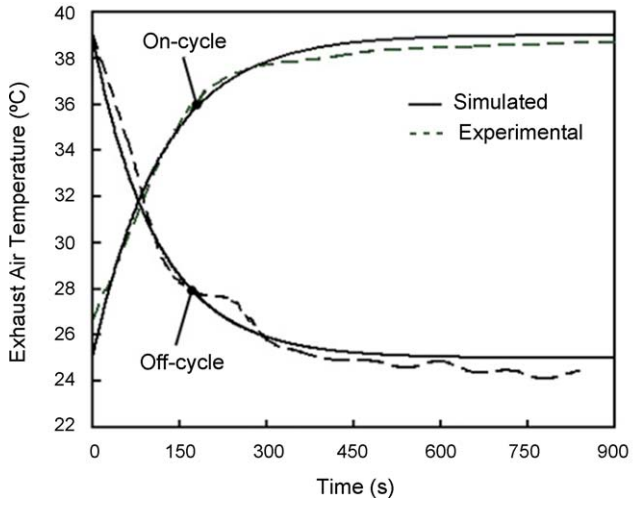

Fig. 5. Comparison of the simulated temperature expression used in the mathematical model with the experimental exhaust air temperature recorded from the fuel cell module for both the on and off-cycles.

the fuel cell is switched on and off and the blower is run at full speed. Presumably this cycle is used to remove excess hydrogen and water. Although the purge cycle is not modelled exactly, the anomalous plateau section is not too severe and the overall trend for the temperature during the off-cycle can be simulated with an exponential expression. This is explained in more detail in the following section.

4. Heat transfer calculations

The thermal coupling between the fuel cell and the metal hydride tanks is a complex scenario which can be approximated by a series of relations describing air temperature and convection coefficients as a function of time. Many assumptions are required to allow for this scenario to be modelled while at the same time adequately representing a real-life application. For heat transfer to and from the metal hydride canisters it is assumed that radiation is negligible and heat transfer is due only to convection. It is also assumed that the exterior of the duct work is insulated and there is no heat transfer between the duct work and the surroundings. For the cases involving ducted flow over the tank it is assumed that during the off-cycle the heat transfer from the exterior tank walls is due only to natural convection with air that is at ambient temperature. It is also assumed that because the tank is physically mounted by the top and bottom surfaces that these surfaces are insulated and heat transfer only occurs through the side wall. For the annular case it is assumed that the exterior tank walls are insulated and during the off-cycle the air through the interior channel is sufficiently quiescent such that minimal heat transfer occurs. Finally, it is assumed that the exhaust air can be described by a first-order response function.

4.1. Fuel cell exhaust air temperature during the on-cycle

In order to model the interaction between the tank and the external air flow, an expression describing the temperature of the exhaust air as it leaves the stack is required. Assuming the behaviour of the air temperature can be approximated as a first-order response function, the transient nature of the air temperature during operation can be described by the following equation:

$$\frac{T_a(t) - T_{ss}}{T_0 - T_{ss}} = \exp\left(-\frac{t}{\tau_{on}}\right) \quad (1)$$

where T_0 is the initial temperature of the air at the start of each on-cycle, T_{ss} the steady-state temperature (∼39 °C), t is time, and τ_{on} is the experimentally determined time constant for the on-cycle (∼120 s). When these values are utilized, Eq. (1) yields a temperature behaviour that corresponds well to the experimental results. This can be seen in Fig. 5 by comparing the simulated temperature curve with the experimental data.

To determine the amount of air flow exiting the fuel cell stack, a comparison is made between the temperature and flow rate values provided in the documentation for rated load versus the values experimentally determined at half load. At rated load (1200 W) and operating temperature the temperature of the exhaust air is listed as 17 °C above ambient temperature, the max flow rate is listed as 3600 SLPM, and the waste heat is given as 1650 W [13]. At half load the temperature difference is 14 °C above ambient temperature, and the waste heat is listed as 550 W. Not all of the waste heat is removed by the exhaust air stream, but using the given data and the measured temperatures, the heat absorbed by the air stream can be estimated. Performing an energy balance using the flow rate and temperature values at rated load yields a value of 1130 W for the heat removed by the air. Utilizing a ratio of actual waste heat (1650 W) and calculated amount of heat removed by the air (1130 W) for full load, the value of heat removed by the air at half load is determined to be 377 W assuming similar thermal behaviour at 50% load. An energy balance performed using this value and the experimental data from above yields a flow rate of 1450 SLPM for the exhaust air at half load.

4.2. Fuel cell exhaust air temperature during the off-cycle

With the exhaust air temperature of the on-cycle determined, the temperature drop during the off-cycle must now be determined. Once the fuel cell has been turned off and the purge cycle is completed, the exhaust fan no longer blows air through the cooling channels; therefore the air within the channels will experience minimal movement and is assumed to be quiescent. Because there is assumed to be no interaction between the fuel cell exhaust air and the metal hydride tanks during the off-cycle there is no need to determine the flow rate through the channels. However, in order to determine the initial temperature, T_0, that is to be used when the fuel cell is turned on again, the drop in air temperature while the fuel cell is turned off for 15 min must be determined. This temperature drop is due to the drop in stack temperature as it exchanges heat with its surroundings. The equation that describes the transient behaviour of the air temperature for the off-cycles is assumed to be similar to Eq. (1) (i.e. a first-order response function); however, the steady-state

temperature is now the ambient air temperature (∼25 °C):

$$T_a(t) = T_\infty + (T_0 - T_\infty)\exp\left(-\frac{t}{\tau_{off}}\right) \quad (2)$$

where T_∞ is the ambient air temperature, and τ_{off} the experimentally determined time constant during the off-cycle (∼110 s). As illustrated by Fig. 5, the simulated temperature profile corresponds well to the experimental data. It is not necessary to implement this expression into the model because the air temperature reaches a steady-state value at ambient temperature within a 15 min (900 s) time period. Therefore, at the start of each on-cycle the initial temperature used in Eq. (1), T_0 is the ambient air temperature (∼25 °C). If a shorter period for the off-cycle was to be simulated, then Eq. (2) would be needed.

4.3. External air temperature for the base and finned cases

The temperature of the exhaust air for the on-cycle has been determined as the air exits the fuel cell cooling channels. However, this information alone is insufficient for the convection heat transfer relations associated with flow past the metal hydride tanks. As the air flows over the exterior of the tanks, the thermal interaction with the tanks causes a decrease in the temperature of the air since energy is transferred from the air stream into the hydride tanks. An average temperature value is required for the convection heat transfer relations, which is calculated as follows:

$$T_{air} = \frac{T_{in} + T_{out}}{2} \quad (3)$$

where T_{in} is calculated from Eq. (1) and Eq. (2) for the on and off-cycles respectively, and T_{out} represents the temperature after the air stream has interacted with the hydride tanks. T_{out} is calculated by simultaneously solving Eq. (3) and the following energy balance, which accounts for the energy transferred to the metal hydride tanks.

$$h_{side}A_{side}(T_{air} - T_{side}) = m_a c_{pa}(T_{in} - T_{out}) \quad (4)$$

where h_{side} is the convection coefficient along the side wall of the tank, A_{side} the area of the side wall, T_{side} the average external temperature of the side wall, m_a the mass flow rate of the air, and c_{pa} is the specific heat capacity of the air stream.

4.4. Air temperature for the annular case

Because the exhaust air flows through a narrow circular duct for the annular case, it experiences a large temperature gradient in the z-direction. A separate subdomain is used to account for the energy transferred to the metal hydride tanks as a function of axial position through the cylinder. Assuming incompressible flow and viscous dissipation is negligible, the equation describing air temperature is as follows:

$$\rho_a c_{pa} A_o \frac{\partial T_{air}}{\partial t} + m_a c_{pa}\frac{\partial T_{air}}{\partial z} = h_{si}P(T_{si}(z) - T_{air}) \quad (5)$$

where ρ_a is the density of the air, A_o the cross-sectional area of the channel, h_{si} the convection coefficient along the interior wall, P the perimeter of the interior channel opening, and T_{si} is the local temperature of the wall at each node along the interior channel of the tank. The inlet value of T_{air}, at $z = 0$ cm, is calculated from Eq. (1) for each on-cycle. During the off-cycle heat transfer through the interior wall is assumed to be negligible; therefore, an expression for the air temperature is not required.

4.5. Convection correlations

The base and finned cases involve a cylinder in cross flow. The average convection coefficient is determined using the correlation due to Hilpert [15]:

$$Nu_D = (0.683)Re_D^{0.466}Pr^{1/3} \quad (6)$$

where Pr is the Prandtl number of the air stream, and the Reynolds number, Re_D, is calculated as follows [15]:

$$Re_D = \frac{\rho_a v_m D}{\mu_a} \quad (7)$$

where v_m is the mean free stream velocity of the air, D the diameter of the tank, and μ_a the dynamic viscosity of the air. This yields a convection coefficient of ∼12.5 W m^{-2} K^{-1} for the base case during the on-cycle.

For the off-cycle, there is no forced air stream; therefore the heat transfer is due to natural convection. The average convection coefficient over the entire circumference of the cylinder is determined using the correlation due to Churchill and Chu [15]:

$$Nu_D = \left\{0.60 + \frac{0.387Ra_D^{1/6}}{[1 + (0.559/Pr)^{9/16}]^{8/27}}\right\}^2 \quad (8)$$

The Rayleigh number, Ra_D, is determined as follows:

$$Ra_D = \frac{g(T_s - T_\infty)D^3}{T_f \nu \alpha} \quad (9)$$

where g is the acceleration due to gravity, T_s the temperature on the surface of the tank, T_f the film temperature ($T_f = [T_s + T_\infty]/2$), ν the kinematic viscosity, and α is the thermal diffusivity. Eqs. (8) and (9) are entered directly into the metal hydride model since the convection coefficient due to natural convection varies as the temperature difference between the tank surface and the ambient air varies. The properties of air for the off-cycle are assumed to be constant at the average film temperature (295 K) and are summarized in Table 1.

The addition of 50 fins should increase the heat transfer significantly. This increase in heat transfer can be accounted for by using an equivalent convection coefficient. This convection coefficient can then be applied to the original geometry of the model, negating the need to model all of the fins separately. An

Table 1
Properties of the air during the off-cycle [15]

Parameter	Value
Thermal conductivity, k (W m^{-1} K^{-1})	2.59×10^{-3}
Kinematic viscosity, ν (m^2 s^{-1})	15.44×10^{-6}
Thermal diffusivity, α (m^2 s^{-1})	21.84×10^{-6}
Prandtl number, Pr	0.7083

Table 2
Properties of the tank wall material, aluminum 2024-T6 [15]

Parameter	Value
Density, ρ (kg m^{-3})	2770
Specific heat, c_p (J kg^{-1} K^{-1})	875
Thermal conductivity, k (W m^{-1} K^{-1})	177

equivalent convection coefficient can be defined using the following equation for overall efficiency of a finned surface [15].

$$h_{\text{fin}} A_{\text{side}} = h_{\text{base}} A_{\text{t}} \left[1 - \frac{N A_{\text{f}}}{A_{\text{t}}} (1 - \eta_{\text{f}}) \right] \tag{10}$$

A_{t} is the total surface area including fins and base, N the number of fins, A_{f} the surface area of each fin, and η_{f} the efficiency of a single fin. The thermal mass of the fins is neglected. The fin efficiency is determined to be 98.5%, which yields an effective convection coefficient of ~170 W m^{-2}K^{-1} during the on-cycle.

For the annular case, the air is flowing through a small circular duct. For fully developed turbulent flow in circular tubes the following correlation can be used [15].

$$Nu_{\infty} = \frac{(f/8) Re_{\text{D}} Pr}{1.07 + 12.7(f/8)^{1/2}(Pr^{2/3} - 1)} \tag{11}$$

where the friction factor, f, is calculated by the following equation for a smooth surface [15].

$$f = 0.184 Re_{\text{D}}^{-1/5} \tag{12}$$

Since the tube is short, $L/D \approx 32$, it cannot be assumed that the turbulent air flow is fully developed. The convection coefficient for the entry region will exceed the convection coefficient for fully developed flow. To account for the entry effects Eq. (11) can be corrected assuming a square-edged entrance as follows [16]:

$$\frac{Nu_{\text{m}}}{Nu_{\infty}} = 1 + \frac{2.4254}{(L/D_{\text{o}})^{0.676}} \tag{13}$$

where Nu_{m} is a mean Nusselt number for the entire length of the tube, D_{o} the diameter of the interior opening, and L the length of the tube. Although Eq. (13) yields a mean Nusselt number, it is assumed that this expression can also be used to approximate the local convection coefficient.

5. Metal hydride model

The mathematical model used to describe the behaviour of the metal hydride is the same as the model utilized by the authors in a previous paper [12]. Here, two additional subdomains are included in addition to the subdomain representing the metal hydride alloy. The first subdomain simulates the tank walls, which are assumed to be 2024 T6 aluminum (properties are summarized in Table 2). This two-dimensional subdomain is shown in Fig. 6a and b as the unshaded region around the exterior of the metal hydride alloy (shaded region). The second subdomain accounts for the transient and spatial variation of the temperature of the exhaust air stream as it passes through the interior tube of the annular case. This one-dimensional subdomain is

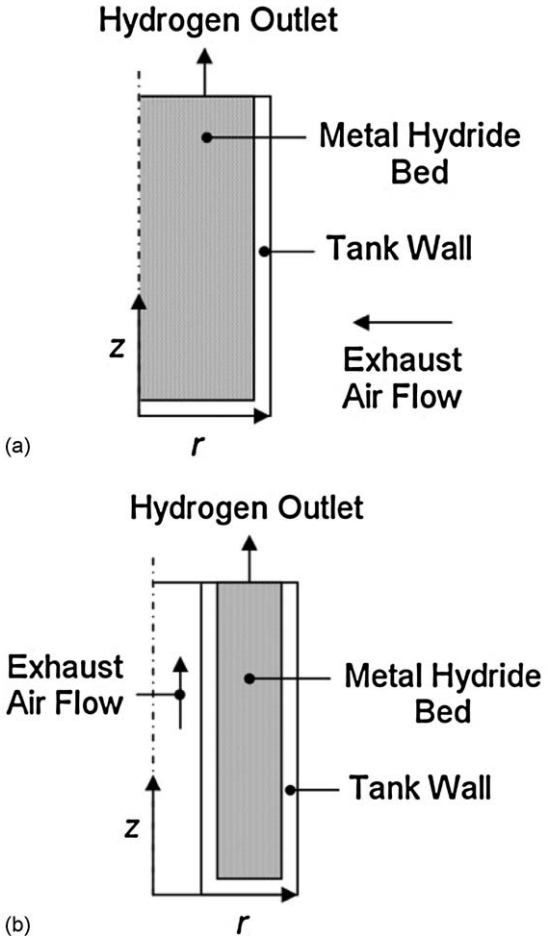

Fig. 6. (a) Schematic of metal hydride tank used in mathematical model for the base and finned cases. (b) Schematic of metal hydride tank used in mathematical model for the annular case.

implemented along the left-hand side of the wall in Fig. 6b, at $r = 0.74$ cm. The subdomain for the metal hydride is the shaded region in Fig. 6a for the base and finned cases, and Fig. 6b for the annular case. For the base and finned cases the outer tank radius is 3.175 cm, the height is 24 cm, and the thickness of the aluminum is 4 mm. For the annular case the outer tank radius is 3.4 cm, the radius of the internal opening is 0.74 cm, the height is 24 cm, and the thickness of the aluminum is 4 mm.

The metal hydride is assumed to be $Ti_{0.98}Zr_{0.02}V_{0.43}Fe_{0.09}Cr_{0.05}Mn_{1.5}$ and the important properties of this alloy are summarized in Table 3. This alloy is assumed to have flat absorption and desorption plateaus on the P–C diagram, and the middle

Table 3
Properties of the metal hydride alloy, $Ti_{0.98}Zr_{0.02}V_{0.43}Fe_{0.09}Cr_{0.05}Mn_{1.5}$

Parameter	Value
Saturated density, ρ_{sat} (kg m^{-3})	5577
Empty density, ρ_{emp} (kg m^{-3})	5500
Specific heat, c_p (J kg^{-1} K^{-1})	490
Effective thermal conductivity, k_{e} (W m^{-1} K^{-1}) (assumed)	1.4
Permeability, K (m^2) (assumed)	10^{-8}
Reaction heat of formation, ΔH° (J kg^{-1})	-1.359×10^7
Porosity, ε (assumed)	0.50

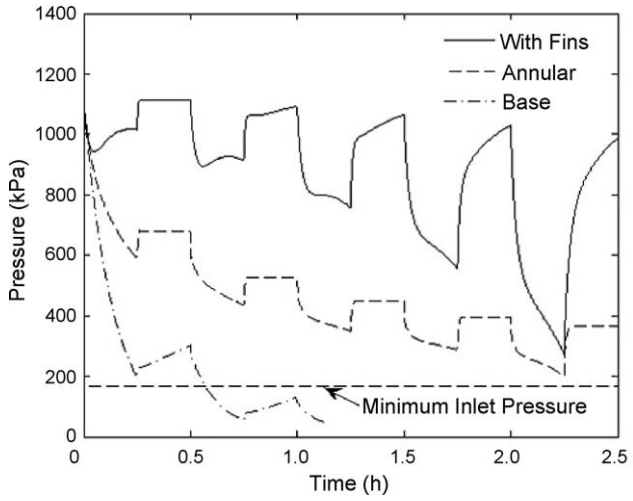

Fig. 7. Hydrogen gas pressure inside the metal hydride tank during the 2.5 h of pulsed operation, showing the comparison between the base, finned, and annular cases. The minimum acceptable inlet pressure to the fuel cell is also shown.

value is used in the equations. Hysteresis is included in the model by utilizing two distinct equations for the absorption and desorption pressures. The model also assumes thermal equilibrium between the hydrogen and metal hydride alloy within the tank.

6. Results and discussion

As described earlier, the dynamic load profile serviced by the fuel cell system is assumed to be a series of on–off step functions lasting for 2.5 h, which is five full cycles. After the five complete cycles approximately 89% of the hydrogen contained in the tank is consumed, as seen in Fig. 1. All three of the cases are subject to the same hydrogen demand load. The performance of the three storage systems is compared by studying the pressure of the hydrogen gas within the tank throughout the 2.5 h of pulsed operation. In order to understand the details of the behaviour within a metal hydride tank three additional plots are generated in addition to the pressure plot; the metal hydride density profile throughout the 2.5 h of operation, the temperature profile during one on-cycle, and a profile of the rate of hydrogen desorption during one on-cycle. Because the base case is only able to provide hydrogen for two complete cycles there is little temporal variation in these parameters, and plots would provide little useful information. Therefore, the three profile plots are generated to compare finned and annular cases only.

6.1. Hydrogen pressure comparison

Fig. 7 shows the average pressure of the hydrogen within the tank for all three cases. Since there is a minimal pressure gradient throughout the tank, the pressure at the centre of the metal hydride domain is used as the average pressure.

The base case is the original tank with no heat transfer enhancements. Fig. 7 shows that for the first two cycles the base case is able to provide hydrogen at the required flow rate. However, the pressure within the tank, and therefore the delivery pressure of the hydrogen is significantly lower than the other two cases. The fuel cell requires a minimum hydrogen inlet pressure of 170 kPa (absolute) as shown in Fig. 7, which the base case cannot maintain during the second on-cycle. During the third on-cycle the base case reaches a pressure of zero, indicating that the dehydriding reaction rate is insufficient to satisfy the demand flow rate although the tank is still ∼60% full. The reason for the decrease in the minimum pressure for each cycle as the tank empties is due to the progression of the reaction zone towards the centre of the tank, and the increasing thermal resistance due to the increasing distance the thermal energy must travel through the hydride bed. This phenomenon is described in more detail in a previous study [12]. Essentially, the desorption is limited by heat transfer, a well-known issue with metal hydride storage systems.

Because the base case is unable to provide the required hydrogen flow, the tank design is modified to enhance the thermal coupling of the fuel cell and the hydrogen storage system. The first modification is the addition of 50 fins along the exterior of the side wall of the tank. Fig. 7 shows that the finned geometry is able to maintain a pressure that is well above that required by the fuel cell. However, the minimum pressure maintained during the on-cycles drops significantly as the tank empties. During the second cycle the pressure is maintained at a minimum value of 950 kPa, while during the fifth cycle the pressure drops to 275 kPa. As noted in the previous paragraph, this decrease is caused by the increasing resistance of the hydride bed. As the dehydriding reaction proceeds away from the external wall the benefits of using fins are reduced. Pressure values that are too high make for a system that must rely more heavily on relief valves for safety or require a thicker tank wall. Other drawbacks to the finned case are the larger volume occupied by the tank due to the external fins and the additional mass associated with the fins. Fig. 4 shows the outer diameter that is required for the finned configuration. Metal hydrides are often used for hydrogen storage in scenarios where size is a key design element, because of the advantageous volumetric capacity. However, if a tank with external fins is used, this advantage is diminished since more space is required. This may not be critical when compared to the base case given the fact that an air flow region is required for the base case as well. A design that limits the volume required for exterior air flow while increasing heat transfer would be preferable. A practical concern with the external fin geometry is the frailty of the finned surface which can be easily damaged, unlike a bare cylinder. Also, the mass of the fins increases the total mass of the hydride tank from approximately 2.2 to 2.9 kg. This is a significant amount especially considering that metal hydride systems already suffer from high mass compared to other hydrogen storage options. Coupling with the fuel cell may require a complicated design of the exterior ducting as well as making it more difficult to interchange tanks. It has also been assumed that the air flow duct is insulated and that all energy interactions are between the tank and the air, which is a scenario that may not be easy to produce. One advantage to this design is the potential ease in manufacturing such a tank. The cylindrical tank can be formed as usual, and a finned sleeve can be inserted on the tank afterwards.

A second method for heat transfer enhancement is to use an annular tank design, and pipe the exhaust air stream from the fuel cell through the central tube. Fig. 7 shows that the annular geometry is able to provide the hydrogen flow rate while maintaining a pressure above the minimum requirement of the fuel cell. The peak pressures in this case are less than the finned configuration, and the variability is also reduced. The minimum pressure maintained during the first cycle is 590 kPa, while the minimum pressure during the fifth on-cycle is 200 kPa. This is an improvement over the 71% reduction experienced for the finned case and is due to the reduced distance the thermal energy must pass through for the annular tank. This shorter radial distance through the hydride bed is illustrated well by Fig. 4. Other advantages of the annular design are the reduced volume and mass, as compared to the finned geometry, and a more robust structure. This configuration also requires a simpler ducting system through the interior tube that would facilitate replacement of the tanks for refuelling. The ducting system for this configuration also ensures that the air stream is isolated from the surroundings and maximum energy exchange is facilitated. One drawback to this design is the possible complexity of manufacturing an annular tank. However, depending on the manufacturing techniques that are employed this may or may not be a more complicated process than the finned tank. Another drawback is the potential for a pressure drop as the air flows through the narrow interior tube that may be too high for the fuel cell exhaust fan. An additional fan may be required to assist with the air flow.

6.2. Metal hydride density profile

Fig. 8 shows the density profile of the metal hydride solid at cross section $z = 12.2$ cm throughout the 2.5 h of operation for the finned and annular cases. The reason for the decrease in metal hydride density as time proceeds is due to the decreasing amount of hydrogen that is part of the solid structure as it is desorbed and released in gaseous form. So Fig. 8 is an indication of the varying hydrogen concentration in the metal hydride bed and therefore the state of fill of the tank throughout the 2.5 h of operation. These profile plots illustrate the different desorption patterns in the finned and annular configurations and specifically display the locations in the tank where desorption takes place as time proceeds.

Fig. 8a shows that the hydrogen is desorbed in a wave-like manner beginning at the exterior wall, where the heat is provided, and proceeds towards the centre of the tank. This accounts for the majority of the gas desorbed. A secondary desorption is also occurring uniformly throughout the tank during certain time intervals. Along the left edge of Fig. 8a, at $r = 0$ cm, it can be seen that as time progresses the density at this point decreases. This indicates that a small amount of hydrogen is being desorbed from the centre of the tank, and not just near the edge. Because of the pulsed square-wave nature of the hydrogen demand, there are short periods where desorption is occurring nearly uniformly throughout the bed where the alloy is not locally depleted. When the hydrogen demand is switched on, the hydrogen gas that has built-up within the tank exits and the pressure drops, creating a low enough pressure within the tank to initiate the desorption reaction throughout the regions in the tank that still contain hydrogen. This more uniform reaction exists momentarily until it is restricted by heat transfer limitations (i.e. the temperature decreases locally, causing the equilibrium pressure, which is temperature dependent, to drop). For the remainder of a period, the reaction dominates in locations where the thermal wave reaches the reaction zone.

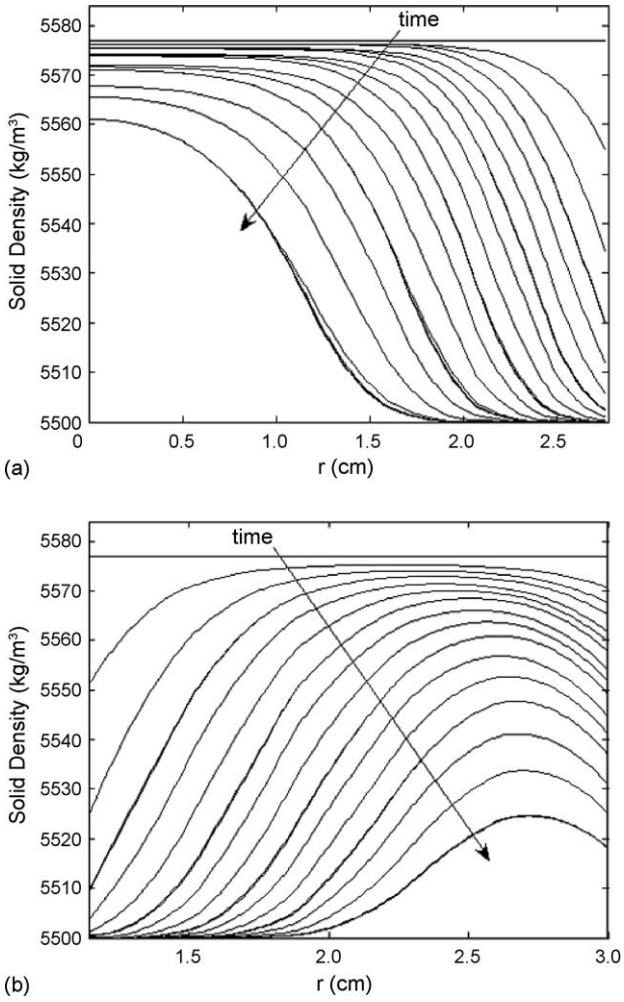

Fig. 8. (a) Density profiles of the metal hydride solid for the finned case at cross section $z = 12.2$ cm for all times ($t = 0$–2.5 h). (b) Density profiles of the metal hydride solid for the annular case at cross section $z = 12.2$ cm for all times ($t = 0$–2.5 h).

Fig. 8b shows a different desorption pattern to that of Fig. 8a due to the annular tank design. In this case the heat is supplied at the centre of the tank, so one would expect the desorption to proceed in a wave-like manner from the centre of the tank to the exterior wall. However, this is not exactly what is observed in Fig. 8b, since there is a significant amount of desorption occurring adjacent to the exterior wall, which is insulated. Due to the high conductivity of the aluminum tank wall, the heat provided at the centre of the tank is able to travel through the bottom of the tank and make its way up the side wall. Therefore, there is an effective heat source along the side wall due to the aluminum, and some desorption occurs. This indicates that the annular configuration benefits from some additional effective

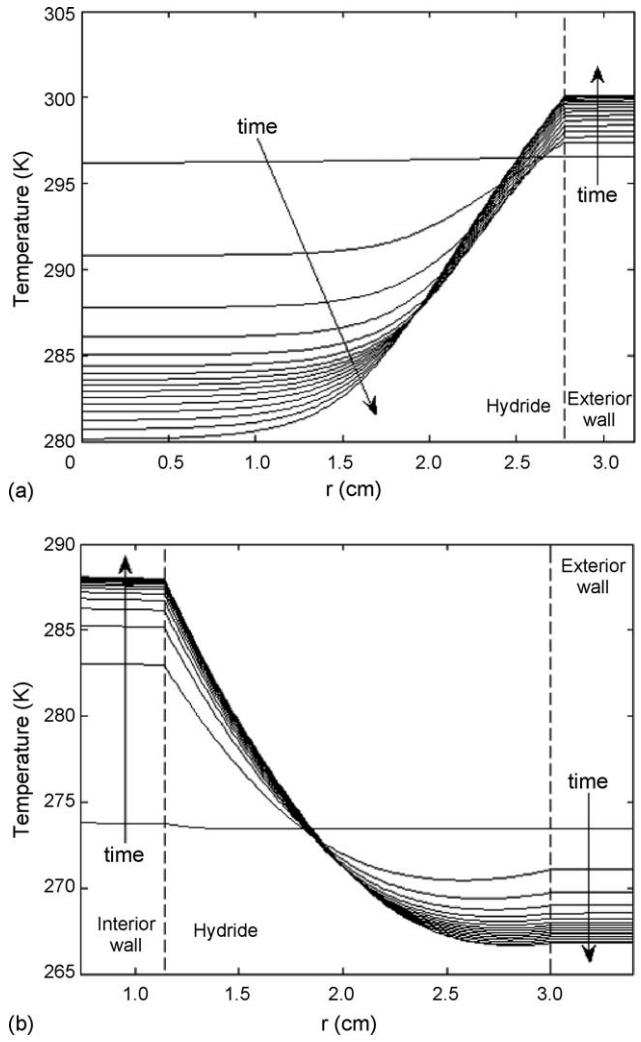

Fig. 9. (a) Temperature profiles for the finned case at cross section $z = 12.2$ cm for one discharge period at times $t = 1.5$–1.75 h. (b) Temperature profiles for the annular case at cross section $z = 12.2$ cm for one discharge period at times $t = 1.5$–1.75 h.

heat sources along the exterior of the metal hydride bed due to the aluminum tank walls. This phenomenon also illustrates the importance of including the aluminum tank wall when modelling different metal hydride tank configurations.

6.3. Temperature profile

Fig. 9 shows the temperature profile of the metal hydride solid at cross section $z = 12.2$ cm for one on-cycle at times $t = 1.5$–1.75 h for the finned and annular cases. The temperature within the tank during cycling is not as uniform as the pressure. It can be seen from Fig. 9 that a bulk average temperature value would have little meaning. Since the energy equation is active in the tank walls these profile plots include the temperatures in the aluminum walls.

Fig. 9a further illustrates the wave-like desorption pattern discussed above for the metal hydride density profile. Heat is provided at the right had side of Fig. 9a, and due to the high conductivity of the aluminum tank wall, the temperature profile is relatively flat in this region. Due to the poor conductivity of the metal hydride bed the temperature profile drops, until the heat reaches the reaction zone. This is located at approximately $r = 1.6$ cm during this cycle, and it can be seen that the energy is not able to pass the reaction zone since the endothermic desorption reaction consumes it; therefore the temperature profile is flat from the reaction zone to the centre of the tank. The temperature along the external wall, at $r = 3.175$ cm, is actually increasing throughout the on-cycle. This is due to the increased heat transfer rate because of the fins. Without any enhancements this temperature would drop and thermal energy would not reach the reaction zone as fast, thus causing a greater pressure drop as observed in Fig. 7. This phenomenon is illustrated in an earlier paper by the authors [12].

Fig. 9b confirms the behaviour described for the metal hydride density profile. In this configuration the heat is provided along the centre wall of the tank at $r = 0.74$ cm. The temperature profile is very similar to that observed for the finned case except that the direction has changed since heat is introduced from the centre and not the exterior wall. The main difference between these two cases is the heat provided by the aluminum wall, seen at $r = 3.0$–3.4 cm in Fig. 9b. Heat energy provided by the side wall can be seen by a small increase in temperature of the metal hydride bed in the alloy adjacent to the wall at this location ($z = 12.2$ cm). At z locations closer to the base, the impact of heat conduction through the wall is greater. Another difference is that the temperature at the beginning of an on-cycle is level at 298.15 K for the finned case and only ~273.5 K for the annular case. This is because the tank in the finned case is exposed to ambient air during the 15 min off-cycle whereas the annular tank is assumed insulated; therefore the finned tank levels off at ambient temperature and the annular tank levels off at a temperature based on a redistribution of the temperature of the system when the off-cycle begins. Because the annular tank begins the on-cycle at a lower temperature, the temperature throughout the demand cycle remains lower than that of the finned tank. This is one reason why the pressures observed for the finned tank are higher than the annular tank. Higher temperatures enable higher pressures, since the equilibrium desorption pressure increases with temperature. These results suggest that allowing thermal interactions with environmental air on the exterior wall of the annular tank should increase performance. Thus, the assumption of an insulated outer boundary is a conservative constraint.

6.4. Hydrogen desorption profile

Fig. 10 illustrates the location along the r-axis where desorption is occurring at cross section $z = 12.2$ cm, for the hydrogen discharge period at times $t = 1.5$–1.75 h. The Y-axis is labelled as hydrogen absorption because the overall desorption term is configured to be positive for absorption and negative for desorption. Therefore, although the Y-axis is labelled as absorption, the values in the plot are negative, indicating that desorption is occurring.

Fig. 10a shows a lower minimum point for desorption than Fig. 10b. The dip in the curves represents the location of the main reaction zone. The finned case therefore has a more concentrated reaction zone due to the higher temperatures and single heat

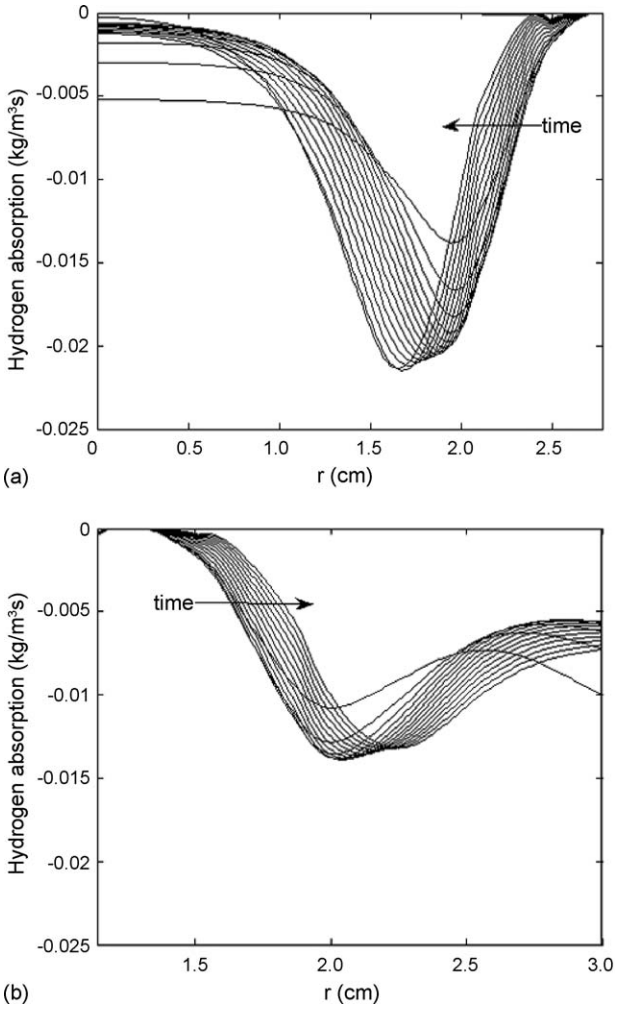

Fig. 10. (a) Profiles of the rate of hydrogen mass being desorbed from the metal hydride bed for the finned case at cross section $z = 12.2$ cm for one discharge period at times $t = 1.5$–1.75 h. (b) Profiles of the rate of hydrogen mass being desorbed from the metal hydride bed for the annular case at cross section $z = 12.2$ cm for one discharge period at times $t = 1.5$–1.75 h.

source (only external wall) as described above. Fig. 10b shows that the annular case does not reach the same magnitude of desorption in any single location as the finned case; however it has a desorption pattern that is more spread out across the radius of the tank. This is due to the additional effective heat source provided by the conductance of heat through the aluminum tank walls that allows desorption to occur within the hydride bed adjacent to the exterior wall at $r = 3.0$ cm.

The metal hydride density, temperature, and hydrogen desorption profiles shed some light into the behaviour of metal hydride tank configurations that are subjected to a pulsed hydrogen demand load. These results reveal complex temperature and pressure behaviour that may enable creative solutions to the heat transfer problem.

7. Conclusions

Thermal coupling of a metal hydride storage system and a fuel cell module was investigated for a specified time-dependent electrical demand. The ability of three different metal hydride tanks to satisfy the minimum hydrogen delivery pressures were simulated and compared. For the dynamic cycle used in this study, the base case (bare cylinder) is unable to service the required flow of hydrogen gas. A tank with 50 external fins meets the required demand however the peak pressure is considerably higher than what is necessary. Furthermore, this configuration satisfies fuel flow requirements but occupies more volume and has a higher mass, which may partially diminish the advantage of using a metal hydride system. The fins are also frail and may be subject to damage. An annular tank design was found to provide hydrogen gas at the required flow rate and pressure stipulated by the fuel cell. The peak pressures in this case are lower than with the finned tank, making the system somewhat safer. The annular tank design requires less volume than a finned design and may be easier to integrate to the fuel cell. The annular configuration also provides a robust design, and a simple ducting system that reduces energy lost to the surroundings. It was found that although the exterior wall in the annular case is assumed insulated, heat conduction through the aluminum from the inner wall to the outer wall helps maintain pressure throughout the operating period.

Acknowledgements

This work was supported by the Natural Sciences and Engineering Research Council of Canada. The authors would like to thank Jordan Roszmann for providing the three-dimensional drawings of the fuel cell and the duct work, and Alvin Bergen and Tom Schmeister for assisting with the testing of the fuel cell module.

References

[1] G. Sandrock, J. Alloys Compd. 293/295 (1999) 877–888.
[2] Z. Jiang, R.A. Dougal, S. Liu, S.A. Gadre, A.D. Ebner, J.A. Ritter, J. Power Sources 142 (2005) 92–102.
[3] S. Mazumdar, S. Bhattacharyya, M. Ramgopal, Int. J. Refrig. 28 (2005) 798–809.
[4] A. Demircan, M. Demiralp, Y. Kaplan, M.D. Mat, T.N. Veziroglu, Int. J. Hydrogen Energy 30 (2005) 1437–1446.
[5] U. Mayer, M. Groll, W. Supper, J. Less-Common Metals 131 (1987) 235–244.
[6] M.R. Gopal, S.S. Murthy, Int. J. Hydrogen Energy 17 (1992) 795–805.
[7] A. Jemni, S. Ben Nasrallah, Int. J. Hydrogen Energy 20 (1995) 43–52.
[8] A. Jemni, S. Ben Nasrallah, Int. J. Hydrogen Energy 20 (1995) 881–891.
[9] S. Ben Nasrallah, A. Jemni, Int. J. Hydrogen Energy 22 (1997) 67–76.
[10] A. Jemni, S. Ben Nasrallah, J. Lamloumi, Int. J. Hydrogen Energy 24 (1999) 631–644.
[11] M. Mat, Y. Kaplan, Int. J. Hydrogen Energy 26 (2001) 957–963.
[12] B. MacDonald, A. Rowe, Int. J. Hydrogen Energy, in press.
[13] BALLARD© Nexa™ Power Module User's Manual (MAN5100078), Ballard Power Systems Inc., 2003.
[14] Ovonic® Solid Hydrogen Storage System Portable Canisters Brochure, Ovonic Hydrogen Systems LLC, 2005.
[15] F.P. Incropera, D.P. DeWitt, Fundamentals of Heat and Mass Transfer, 5th ed., John Wiley and Sons, New York, 2002.
[16] M.S. Bhatti, R.K. Shah, in: S. Kakaç, R.K. Shah, W. Aung (Eds.), Handbook of Single-Phase Convective Heat Transfer, John Wiley and Sons, New York, 1987, pp 4.1–4.166.